Volume 1 | Number 1 | Jan 2013 | Pages 1–100

Journal of
Materials Chemistry A

Materials for energy and sustainability
www.rsc.org/materialsA

Li⁺

ROYAL SOCIETY OF CHEMISTRY

ROYAL SOCIETY OF CHEMISTRY

www.rsc.org/materialsA

Journal of Materials Chemistry A

ARTICLE

A hybrid photoelectrode with plasmonic Au@TiO$_2$ nanoparticles for enhanced photoelectrochemical water splitting

Piangjai Peerakiatkhajohn,[a] Teera Butburee,[a] Jung-Ho Yun,[a] Hongjun Chen,[a] Ryan M. Richards[b] and Lianzhou Wang[a]*

Herein we present a new p-n heterojunction photoelectrode design utilizing Cu$_2$O and TiO$_2$-P25 loaded with only 1 wt% Au@TiO$_2$ plasmonic core-shell structure for the photoelectrochemical (PEC) process. It is found that the photoelectrode with a sandwich-like layer design, i.e. TiO$_2$-1wt% Au@TiO$_2$/Al$_2$O$_3$/Cu$_2$O, not only promotes light harvesting but also improves charge carrier separation, resulting in drastically improved photocurrent density up to -4.34 mA·cm^{-2} at -0.2 V vs. Ag/AgCl under simulated AM 1.5 solar illumination, ~20 fold enhancement compared to that obtained from a TiO$_2$-P25/Cu$_2$O photoelectrode. It is also revealed that the photoelectrochemical performance is closely related to the Au nanoparticle size, induced by surface-enhanced scattering of the plasmonic nanoparticles. It should also be noted that these multilayer photoelectrodes also exhibit high stability through rational design of the PEC system to avoid the photocorrosion on Cu$_2$O layers.

Introduction

Solar energy is considered as an ideal renewable energy source that could facilitate global sustainability.[1, 2] The photoelectrochemical (PEC) system in particular can be considered as a promising solar energy conversion technology that can directly convert solar light energy into the chemical fuel such as hydrogen through water splitting process.[3, 4] The efficiency of PEC water splitting is dependent on light absorption and charge separation/transportation /recombination processes, which are dependent on the photoelectrode design in the PEC system.[5-8] As a representative photoelectrode material, TiO$_2$ is a reliable photocatalytic semiconductor with high stability. A vast amount of studies have been concentrating on the performance improvement of TiO$_2$-based photoelectrodes by modifying its crystalline structure, shape and size, doping with metals/non-metals, or coupling with other semiconductors and metals.[9-12] In particular, the modification of TiO$_2$ photoelectrodes by coupling narrow band gap semiconducting materials has been considered to be one of the effective approaches in extending light absorption of the UV-light active TiO$_2$ photoelectrodes to the visible region. Among the coupled semiconducting materials in TiO$_2$ based PEC systems, cuprous oxide (Cu$_2$O) is a promising candidate owing to the features of the small band gap energy of ~ 2.1 eV, a high theoretical photocurrent density of -14.7 mA·cm^{-2}, non-toxicity, and low-cost.[13-15] However, the Cu$_2$O layer in the photoelectrodes can easily be decomposed by photocorrosion during PEC reactions. To protect Cu$_2$O, Cu$_2$O@TiO$_2$

core-shells and Cu$_2$O/TiO$_2$ bi-layered heterojuction structures have been designed.[13, 16-18] Recently, Grätzel and co-workers reported one type of Cu$_2$O based photoelectrodes which were decorated by Al-doped ZnO and TiO$_2$ multi-protecting barrier layers, which delivered a cathodic photocurrent density up to -7.6 mA·cm^{-2}.[13] However, the atomic layered deposition (ALD) technique employed to form the Al-ZnO/TiO$_2$ protecting barrier layer in their work have the concerns of high fabrication cost and the difficulty of scale-up.

Herein, we report a new class of sandwich-like TiO$_2$-1 wt% Au@TiO$_2$/Al$_2$O$_3$/Cu$_2$O photoelectrodes using a simple low-cost solution based process. The incorporation of a small amount of Au core/TiO$_2$ shell (Au@TiO$_2$, 1 wt%) in the TiO$_2$-P25 layer offers synergistic effects in plasmonic-assisted light absorption improvement, enhanced charge separation rate and protection of the Cu$_2$O layer against photocorrosion. In addition, an insulating Al$_2$O$_3$ layer was inserted between TiO$_2$-1 wt% Au@TiO$_2$ and Cu$_2$O in order to improve the interfacial charge separation. The back-illumination on the newly designed PEC simultaneously improves the stability of the electrodes as well as facilitating charge separation and transport processes via the efficient electric field induced by the interfacial layers of the heterojunction photoelectrodes.

Experimental

Copper sulphate, tetrachloroaurate (III) hydrate (HAuCl$_4$·3H$_2$O), cetyltrimethylammonium bromide (CTAB) and mercaptoacetic acid were purchased from Sigma-Aldrich. Titanium (III) chloride was purchased from Alfa Aesar. Lactic acid and nitric acid were purchased from Australia Supplier Company. All reagents used in this experiment were analytical grade without further purification. Conductive fluorine-doped tin oxide (FTO, 10×40×2.3 mm, 15Ω/sq, Dyesol Glass) glass substrates were used for all working electrodes. Milli-Q water (18.2 MΩ) was used throughout the experiments.

Preparation of Au@TiO$_2$ nanostructure thin film electrodes

[a] Nanomaterials Centre, School of Chemical Engineering and Australian Institute for Bioengineering and Nanotechnology, The University of Queensland, St Lucia, QLD,4072, Australia. E-mail: l.wang@uq.edu.au
[b] Department of Chemistry and Geochemistry, Colorado School of Mines, Golden, CO 80401, USA. National Renewable Energy Laboratory, Golden, CO 80401, USA
Electronic Supplementary Information (ESI) available: [SEM images, UV-Vis spectra PEC measurement and Stability test]. See DOI: 10.1039/x0xx00000x

The Au metal cores were synthesized by using seed-mediated process according to previous reports.[19, 20] The well-defined Au@TiO2 structures were prepared by the method developed by Butburee et. al.[21] Briefly, 500 mL of the as-prepared Au solution was centrifuged at 4500 rpm for 15 minutes, followed by decanting and re-dispersion in 50 mL water. These centrifuge and re-dispersion processes were repeated 3 times. Then, 50 mL of 50 mM mercaptoacetic acid was added with mechanical stirring over 12 hours to modify the surface of the metal nanoparticles to be selective for TiO2 deposition. After surface modification, the pH of both the Au-core solution and 10 mL of 0.5 M TiCl3, which was used as the precursor of TiO2 shell, were adjusted to 2.75. Then, 0.5 mM TiCl3 precursor was added to the Au core solution with stirring. The pH of the reaction was maintained at 2.75±0.05 throughout the reaction by dropping 0.1 M NH4OH when the pH decreased. After the desired reaction time for appropriate TiO2 shell thickness, the solution was centrifuged immediately to stop the reaction and the top aliquot was decanted to remove the excess TiCl3 precursor. The particles were re-dispersed in water and centrifuged for 3 cycles before drying at 60 °C in vacuum oven for 24 hours. For preparation of Au@TiO2 paste, 10 mg of Au@TiO2 nanoparticles was mixed with 1g of TiO2-P25 Degussa powder, 20 mL ethanol, 100 μL of acetic acid and 1 mL of DI water. Subsequently, 4 g of terpineol and 6 g of 10 wt% ethyl-cellulose (pre-dissolved in ethanol) were added. Evaporation of ethanol was performed by a rotary-evaporator with pressure of 120 mbar at a constant bath temperature of 50 °C. The Au@TiO2 paste was then casted on the FTO glasses by doctor-blade method. After paste casting, the resultant photoelectrodes were dried at 100 °C for 15 min and then annealed at 450 ºC for 15 min with a heating rate of 2 °C /min.

TiO2-1 wt%Au@TiO2/Al2O3/Cu2O photoelectrodes

TiO2-1 wt% Au@TiO2/Al2O3/Cu2O photoelectrodes were prepared by designing an Al2O3 ultra-thin layer between the layer of Cu2O and Au@TiO2 using the spin-coating technique. The Al2O3 solution was prepared by dissolving 0.1 M aluminum isopoproxide as a precursor in 50 mL of isopropanol with 2 mL of nitric acid. Then, a thin layer of Al2O3 was deposited on the as-prepared Au@TiO2 layer and heated at 110 °C for 10 min. Next, the top Cu2O thin film was electrodeposited onto the Al2O3/Au@TiO2 electrode in a solution consisting of 0.4 M cupric sulfate and 3M lactic acid (LA) as described the previous report.[2, 22] The pH of the solution was adjusted to 11 by addition of 4 M NaOH solution, and a dark blue solution was obtained under constant stirring. The electrodeposition was carried out in a simple three-electrode cell by using electrochemical workstation (CHI 660D) with an applied potential of −0.4 V (versus Ag/AgCl) at 50 °C for 15 min. The electrode preparation and PEC measurement setup are schematically shown in Fig.1.

Characterization

The Au@TiO2 core-shell structures were characterized using Transmission Electron Microscope (TEM, JEOL 1010) while surface morphologies of the thin films were characterized by using scanning electron microscope (SEM, JEOL JSM-7001F). X-ray Diffraction (XRD) patterns were obtained on XRD spectrometer (Rigaku

Miniflex with cobalt-Kα radiation) at 2θ angle between 20° and 80°. Optical absorption was carried out in the range 300 to 800 nm with a Shimadzu UV-2450 UV-Vis spectrophotometer.

Photoelectrochemical experiment

The photoelectrochemical measurements were performed in a standard three-electrode photoelectrochemical cell on a CHI 660 electrochemical workstation (CH Instruments). An Ag/AgCl and a Pt plate were used as the reference and counter electrode, respectively and an aqueous solution containing 0.1 M Na2SO4 (pH 8.5) was used as the electrolyte. To standardize the results, the photocurrent was measured under solar AM 1.5G illumination (100 mW·cm^{-2}) using a Xenon lamp (150 W, Newport). The illumination area was set by an aperture to 0.785 cm^2. All photoelectrochemical experiments were performed at room temperature and purged with nitrogen gas for 30 min prior to the electrochemical tests.
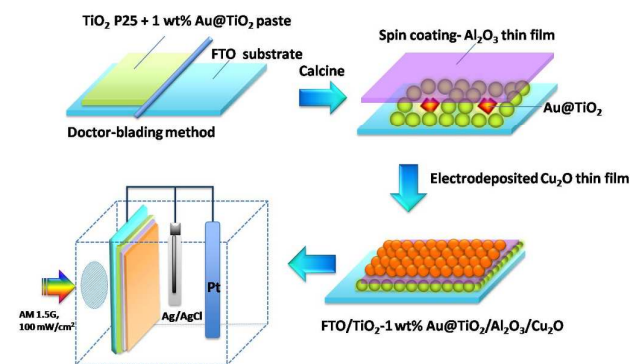

Fig.1. Schematic illustration of the fabrication procedure and PEC measurement setup for TiO2-1 wt% Au@TiO2/Al2O3/Cu2O photoelectrodes.

Results and discussion

Fig. 2A shows the TEM images of concave Au@TiO2 plasmonic nanoparticles with different Au metal core sizes of 37, 70, 100 and 120 nm. The surface TiO2 coating layers are visible based on the contrast difference in the images. The SEM cross-section image of the TiO2-1 wt% Au@TiO2/Al2O3/Cu2O photoelectrode (Fig. 2B) indicates that three heterojunctions are formed into the structured thin films with thickness of approximately 3.5 μm. It is also shown that the Cu2O and Al2O3 layers have completely covered the TiO2-1 wt% Au@TiO2 layer. Here, the transparent Al2O3 layer reveals an extremely smooth thin film with a thickness around 100 nm that should be beneficial for the interfacial charge separation between Cu2O and TiO2-1 wt% Au@TiO2 layer. TiO2-1 wt% Au@TiO2 layer fabricated by a doctor blading technique exhibits a homogenous nanostructured thin film consisting of particles around 20 nm diameter, while the nanospherical particles of electrodeposited Cu2O photoelectrode were larger, with an average size of 70 nm (ESI Fig. S1). The crystal structure of TiO2-1 wt% Au@TiO2/Al2O3/Cu2O photoelectrodes were revealed by X-ray diffraction patterns (Fig. 2C). The XRD patterns of the calcined Cu2O thin film samples at 500 °C in nitrogen gas condition show typical crystalline phase of Cu2O (JCPDS no. 34-1354) with 29.98° (110), 37.0° (111), 42.61° (200), 62.44° (220) and 74.40° (311). The peaks at 25.28°, 53.89°, 55.06°, 62.60°, 68.76 ° and 70.30° are (101), (105), (211), (204), (116) and (220) crystalline planes, respectively, indicating the

ARTICLE

anatase phase, while a peak at 27.38° fits well with the (110) plane indicating rutile phase of TiO_2. The XRD pattern of a bare TiO_2-P25 photoelectrode shows both anatase (JCPDS no. 21-1272) and rutile phases (JCPDS no. 21-1276) with a mixture of 80% anatase and 20% rutile. Meanwhile, the characteristic peaks of Au at 38.1° (111), 44.39° (200) and 77.54° (311) are in good agreement with the JCPDS no. 04-0784. Two small diffraction peaks identified at 37.60° (311) and 45.78° (400) can be indexed to the cubic structure of γ-Al_2O_3 (JCPDS no. 29-0063).
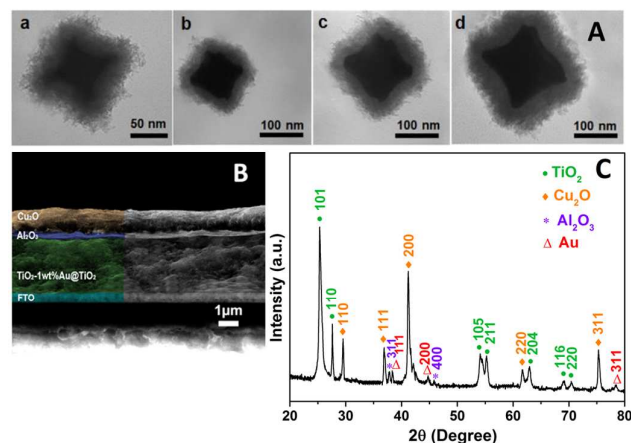

Fig. 2 (A) TEM images of concave Au@TiO_2 core-shell nanoparticles with different sizes of Au cores: (a) 37 nm (b) 70 nm (c) 100 nm and (d) 120 nm. (B) Cross-sectional SEM image of FTO/TiO_2-1wt% Au@TiO_2/Al_2O_3/Cu_2O photoelectrodes (Scale bars: 1 μm) and (C) XRD pattern for FTO/TiO_2-1 wt% Au@TiO_2/Al_2O_3/Cu_2O photoelectrode.

UV-Vis spectra are used to characterize the optical absorption of all of the samples in the range of 300–800 nm, as shown in Fig. 3. The UV-Vis absorption spectra of the photoelectrodes indicate that the light absorption spectra of TiO_2-1wt% Au@TiO_2/Al_2O_3/Cu_2O photoelectrodes increased and red-shifted with an increase in the particle size of the Au core (ESI Fig.S2), and the sample prepared with 120 nm Au core exhibited the highest light absorption. The absorption edge of TiO_2-P25 is around 380 nm, while the absorption band is in the range of 500-700 nm with the maximum absorption at 533.4 nm, we attribute this to both interband transitions and surface plasmon excitation of Au plasmonic metal core.[21] Another absorption band edge around 620 nm is detected, which results from the Cu_2O in heterojunction photoelectrodes. To clarify the possible blocking effect of TiO_2 thin layer, Fig. S3 A presents the optical transmittance spectra. It is evident the transmittance of TiO_2-P25 photoelectrode reaches 80 % in visible region, indicating that the TiO_2 thin film is semi-transparent and absorbs mainly UV light. On the other hand, the FTO/TiO_2-1 wt% Au@TiO_2 exhibits considerably decreased transparency in visible light region. Based on these results, it is reasonable to state that despite some blocking effect of the TiO_2 thin film (semi-transparent), the visible light induced excitation of Au NPs has clear contribution to light absorption and subsequent PEC performance improvement (Fig. S3 B). Note that the broad absorption peak of plasmonic Au nanoparticles containing electrodes is attributable to its core-shell structures in which metal cores are surrounded by higher dielectric materials.[21]

The amperometic curves were collected under chopped light illumination at -0.2 V versus Ag/AgCl in the presence of 0.1 M Na_2SO_4 electrolyte. All TiO_2-1 wt% Au@TiO_2 samples exhibited anodic photoresponse with the highest photocurrent density of 0.6 mA·cm^{-2} observed on the photoelectrode with the 120 nm Au core (ESI Fig. S4). Interestingly, cathodic photoresponses appeared when TiO_2-1 wt% Au@TiO_2 combined with Cu_2O phototelectrode (see ESI Fig.S5 a-b). The photocurrent densities gradually increased with increasing particle size of Au cores.
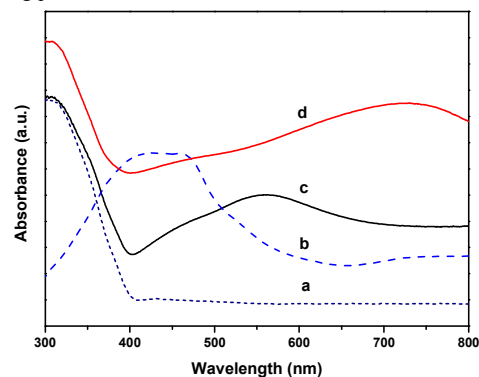

Fig. 3 UV–vis absorbance spectra of various photoelectrodes (a) FTO/TiO_2-P25 (b) FTO/Cu_2O (c) FTO/TiO_2-1wt% Au@TiO_2 (120nm) and (d) FTO/TiO_2-1 wt% Au@TiO_2(120nm) /Al_2O_3/Cu_2O photoelectrodes.
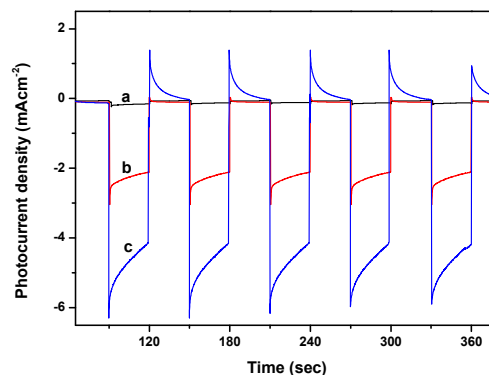
Fig. 4 Amperometic I-t curves of (a) FTO/TiO_2-P25/Cu_2O, (b) FTO/TiO_2-1 wt% Au@TiO_2 (120nm) /Cu_2O, and (c) FTO/TiO_2-1 wt% Au@TiO_2 (120nm) /Al_2O_3/Cu_2O photoelectrodes, collected at -0.2 V vs. Ag/AgCl, respectively under AM 1.5G, 100 mW/cm^2.

Note that all photoelectrodes containing 1wt% Au@TiO_2 exhibited much higher photocurrent density than that of the TiO_2-P25/Cu_2O photoelectrode. Furthermore, the TiO_2-1 wt% Au@TiO_2 (120 nm)/Al_2O_3/Cu_2O photoelectrode exhibits the maximum photocurrent density of -4.34 mA·cm^{-2}, ~20 folds enhancement compared to that of TiO_2-P25/Cu_2O (Fig. 4). The trends in photocurrent densities are in good alignment with the above light absorption spectra, suggesting SPR effects occur in the charge-transfer process. More importantly, the photocurrent densities enhanced 3-folds by introducing the Al_2O_3 thin film, inferring this layer plays an important role in the interfacial charge-separation process.

The fundamental mechanism of TiO_2-1 wt% Au@TiO_2/Al_2O_3/Cu_2O photoelectrode was tentative deduced based on the incident photon-to-current efficiency (IPCE) result. Fig. 5 (A) presents the IPCE

Journal of Materials Chemistry A
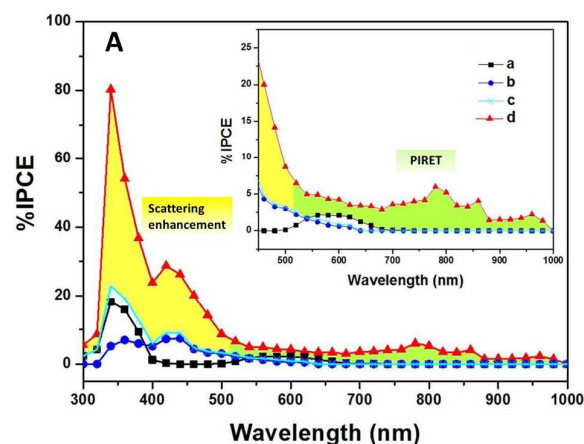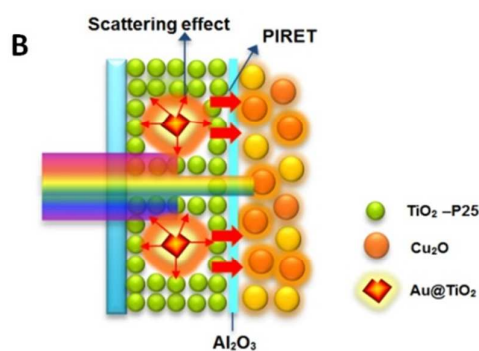
ARTICLE

Fig. 5 (A) Measured incident-photon-to-current efficiency (IPCE) spectra of various photoelectrodes (a) FTO/TiO₂-1 wt% Au@TiO₂ (120 nm) (b) FTO/Cu₂O (c) FTO/TiO₂-P25/Cu₂O and (d) FTO/TiO₂-1 wt% Au@TiO₂ (120 nm)/Al₂O₃/Cu₂O photoelectrodes at an applied bias of -0.2 V vs Ag/AgCl (Inset image represents the measured IPCE spectra with wavelength in range of 450-1000 nm and

(B):Schematic illustration of the photon utilization of the FTO/TiO₂-1 wt% Au@TiO₂/Al₂O₃/Cu₂O photoelectrode.

spectra of each electrode measured in 0.1 M Na₂SO₄ electrolyte under monochromatic illumination as a function of incident photon wavelength. To verify the measurement accuracy, the IPCE result of the FTO/TiO₂-1wt% Au@TiO₂ (120nm)/Al₂O₃/Cu₂O photoelectrode was integrated with AM1.5 solar spectrum and the calculated photocurrent density was ~3.95 mA/cm², which is agreement with the photocurrent measurement results.

The IPCE value of Cu₂O becomes almost zero at 620 nm, corresponding to light absorption spectra and confirming the band gap of 2 eV. In comparison to the TiO₂-P25/Cu₂O photoelectrode, the IPCE spectra of TiO₂-1 wt% Au@TiO₂/Al₂O₃/Cu₂O photoelectrode revealed an enhancement in UV and visible-light near IR region. We can infer that two possible mechanisms, namely scattering effect and plasmonic effect, play roles in this phenomenon. Meanwhile, light scattering provided harvesting light to generate the enhancement on the contacted Cu₂O layer. Basically, a significant proportion of scattered light can be trapped in the semiconductor by reflecting between its top and bottom surfaces.[16,23] Fig. 5 (B) displays the light is preferentially scattered and trapped into the semiconductor TiO₂ by multiple and high-angle scattering was found when TiO₂-1 wt% Au@TiO₂ as first absorbed layer in heterojunction photoelectrode. Another enhancement in visible range near IR region can be attributed to the plasmonic-induced resonant energy transfer (PIRET) effect and the subsequent energy transfer to the semiconductor.[9, 23, 24] The Au metal cores serve as

nano-antennas and capture the energy of plasmon resonance in this region, resulting in enhanced IPCE value between 500 and 980 nm. Furthermore, the large Au plasmonic metal nanoparticles (120 nm) not only have strong surface plasmon resonance but also exhibit preferential incident light scattering into the Cu₂O layer. It can be clearly seen in Fig. S2, the light absorption spectra of FTO/TiO₂-1 wt% Au@TiO₂ was increased and extended to visible light and near IR region when the Cu₂O layer was introduced to the electrode. This

phenomenon confirms a positive contribution from coupling between the localized surface plasmon and semiconductors in this heterojunction photoelectrode design. Obviously, the variation of photocurrent densities of these photoelectrodes as a function of Au@TiO₂ particle size indicates the larger plasmonic nanoparticle size typically leads to more electrons in the SPR state as compared to the smaller plasmonic nanoparticle size.[25, 26] A localized surface plasmon is a collective oscillation of free electrons, typically in a plasmonic metal for which the particle is much smaller than the photon wavelength.

Considering the plasmonic characteristics of the Au@TiO₂ electrodes combining with the p-type Cu₂O photoelectrodes via the thin Al₂O₃ interface film, the heterojunctioned TiO₂-1 wt% Au@TiO₂/Al₂O₃/Cu₂O photoelectrode system can be explained in terms of the charge transport property. Fig. 6 presents the mechanism and charge separation on the TiO₂-1 wt% Au@TiO₂/Al₂O₃/Cu₂O heterostructures photoelectrode in the PEC system. This sandwich-like photoelectrode is mimicking a Z-scheme

type structure PEC cells with effective charge carrier processes. Typically, the Z-scheme provides ohmic contact as the valence band edge of p-type photocathode is close to or lower than the conduction band edge of n-type photoanode.[27, 28] In our Z-scheme like structure, the photogenerated electrons at the conduction band of TiO_2-1 wt% Au@TiO_2 thin film and holes at the valence band of Cu_2O layer tend to recombine in Al_2O_3 interface layer, resulting in H_2 and O_2 evolutions driven by two separate photoelectrodes. In this case, the thin Al_2O_3 layer as an interfacial layer has the function of accelerating charge carrier separation, which subsequently leads to improved H_2 and O_2 evolution process on the electrodes. Therefore, this type of multi-layered photoelectrodes exhibits the cathodic photocurrent and charge transportation in the PEC system that differs from other TiO_2/Cu_2O systems (the traditional charge-carrier transfer mechanism.[8, 16, 17, 29, 30] but demonstrates similar function of Z-scheme system with improved PEC performance for solar fuel generation.[27, 31, 32]
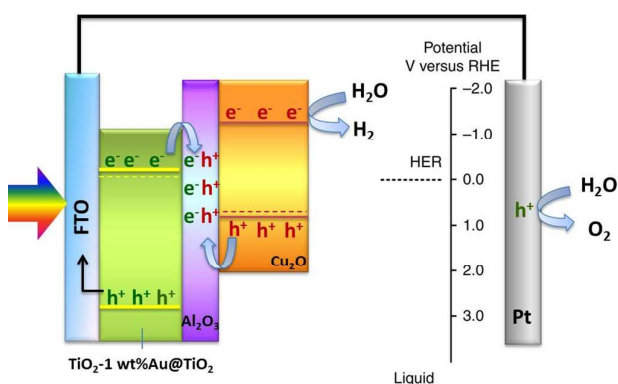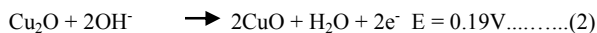

Fig. 6 Schematic diagram of excitation and separation of electrons and holes on TiO_2-1 wt% Au@TiO_2/Al_2O_3/Cu_2O heterostructure photoelectrodes in PEC system.

More interestingly, the internal electric field is supposed to exist in these multi-layered photoelectrodes that provide the synergistic effects for efficient charge separation and stability improvement in these Z-scheme tandem photoelectrodes. The mechanism of photocorrosion presents a redox reaction favoured by thermodynamic condition as summarized in Equations (1) and (2). The photo-generated charges react with Cu_2O directly; electrons reduce Cu_2O to Cu and holes oxidize Cu_2O to CuO.[33]

$$Cu_2O + H_2O + 2e^- \rightarrow 2Cu + 2OH^- \qquad E = 0.05 \text{ V} \ldots\ldots..(1)$$

$$Cu_2O + 2OH^- \rightarrow 2CuO + H_2O + 2e^- \quad E = 0.19V \ldots\ldots..(2)$$

Then, the photocorrosion of photoelectrodes was confirmed with cyclic voltammetry (CV) in the dark scan in the 0.1M Na_2SO_4 electrolyte as shown in Fig. 7 (A). The bare Cu_2O electrode exhibits both cathodic reduction and anodic peaks at around -0.4 V and 0.4 V vs. Ag/AgCl, respectively. Typically, the anodic peak corresponds to the oxidation of Cu_2O to CuO while the cathodic peak corresponds to the reduction of Cu_2O to Cu. On the contrary, the low oxidation peak of TiO_2-1 wt% Au@TiO_2/Al_2O_3/Cu_2O multi-layered photoelectrodes presents photocorrosion resistant behavior

as compared to the bare Cu_2O.

In addition, a comparison for PEC stability of both photoelectrodes can be seen in ESI Fig.S6. As seen in Fig. 7 (B), the long-term stability test for 5 h of Cu_2O and TiO_2-1wt% Au@TiO_2/Al_2O_3/Cu_2O photoelectrodes under illumination show the photocurrent of the Cu_2O photoelectrode is less stable than that of TiO_2-1 wt% Au@TiO_2/Al_2O_3/Cu_2O photoelectrode.
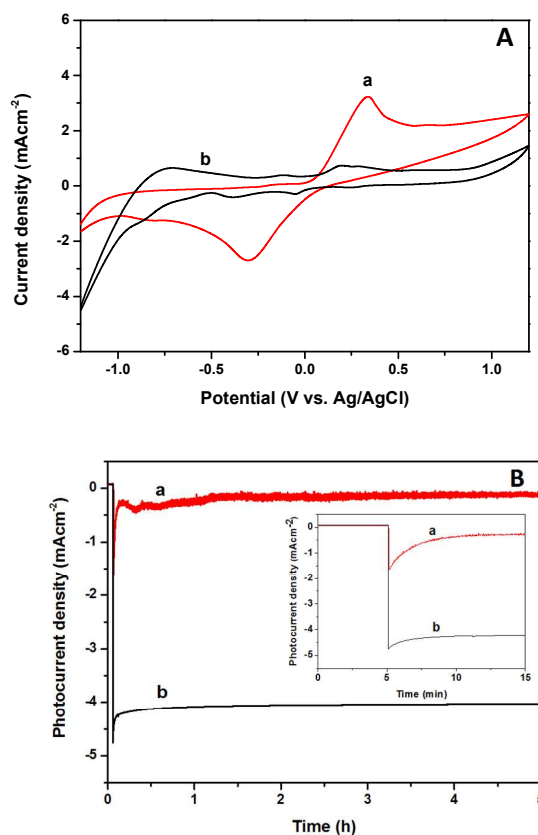

Fig. 7 (A) Dark cyclic voltammograms after 1 h PEC stability measurement and (B) The long-term stability test of (a) FTO/Cu_2O and (b) FTO/TiO_2-1 wt% Au@TiO_2 (120 nm)/Al_2O_3/Cu_2O photoelectrodes with applied potential -0.2 V vs. Ag/AgCl in presence of 0.1 M Na_2SO_4 under AM 1.5 light irradiation. (Inset image shows the photocurrent decay of both photoelectrodes after 15 minutes.

The photocurrent of bare Cu_2O photoelectrode gradually decreases within 1 hour, inferring the photocorrosion behavior. In contrast, the photocurrent density of TiO_2-1 wt% Au@TiO_2/Al_2O_3/Cu_2O photoelectrode is stable at -4.34 mA·cm^{-2} for 5 h under continuous illumination corresponding to the dark cyclic voltammogram result as shown in Fig. S6. This shows the photoelectrode stability of the bare Cu_2O and TiO_2-1 wt% Au@TiO_2/Al_2O_3/Cu_2O photoelectrodes before and after the PEC stability measurement for 1 h in the presence of 0.1 M Na_2SO_4. After the PEC stability test, the bare Cu_2O photoelectrode exhibits decreasing of the anodic peak whereas the multi-layer photoelectrodes reveal the trend similar to the prior PEC stability measurement. As can be seen in the inset photo of bare Cu_2O photoelectrode, a black circle in the illuminated area appeared after the PEC measurement for 1 hr. We describe these

ARTICLE   Journal Name

phenomena by the mechanism diagram shown in Fig. 6, the internal electric field in the multi-layered photoelectrodes effects the charge separation, resulting in an enhancement of the PEC performance. Meanwhile electrons at the conduction band of TiO_2-1 wt% Au@TiO_2 electrode are recombined with the holes remaining at the valence band of the Cu_2O electrode. Due to this recombination on the interfacial layer, photo-generated holes are scavenged, leading to suppressed photocorrosion and increased stability of the photoelectrodes. Therefore, it can be confirmed that the presence of the 1 wt% of Au@TiO_2 can be protective which not only increases the photocurrent density but also the long-term stability in PEC system.

Conclusions

The TiO_2-1 wt% Au@TiO_2/Al_2O_3/Cu_2O photoelectrodes were successfully fabricated using an inexpensive and facile method. The introduction of 1 wt% of Au@TiO_2 nanoparticles not only increases the photocurrent density but also extend the absorption in wide range of the solar spectrum. The Au metal nanoparticles can be used to absorb photons and then transfer the energy to the adjacent TiO_2 and Cu_2O semiconductors. It is also found that the particle size of the Au has dramatic influence on the photocurrent density in photoelectrodes. Of the sizes examined, the photoelectrodes with Au metal cores of 120 nm achieved the highest photocurrent density value (-4.34 mA·cm^{-2}) with more effective plasmonic properties when compared to other TiO_2-P25/Cu_2O studies. From this study and its predecessors it is believed that, plasmonic nanoparticles may be leveraged to address the challenges associated with PEC hydrogen production; especially semiconductors with inadequate light absorption. Moreover, the high efficiency and long-term stability in this multi-layered design can be attributed to the effective separation of the photogenerated charge carriers as Z-scheme PEC device.

Acknowledgements

Notes and references

1. C. X. Kronawitter, J. R. Bakke, D. A. Wheeler, W.-C. Wang, C. Chang, B. R. Antoun, J. Z. Zhang, J. Guo, S. F. Bent, S. S. Mao and L. Vayssieres, *Nano Letters*, 2011, **11**, 3855-3861.
2. T. Jiang, T. Xie, W. Yang, L. Chen, H. Fan and D. Wang, *The Journal of Physical Chemistry C*, 2013, **117**, 4619-4624.
3. X. Zong, S. Thaweesak, H. Xu, Z. Xing, J. Zou, G. Lu and L. Wang, *Physical Chemistry Chemical Physics*, 2013, **15**, 12314-12321.
4. M. Gratzel, *Nature*, 2001, **414**, 338-344.
5. R. M. Navarro Yerga, M. C. Álvarez Galván, F. del Valle, J. A. Villoria de la Mano and J. L. G. Fierro, *ChemSusChem*, 2009, **2**, 471-485.
6. J. Gan, X. Lu and Y. Tong, *Nanoscale*, 2014, **6**, 7142-7164.
7. R. Abe, *Journal of Photochemistry and Photobiology C: Photochemistry Reviews*, 2010, **11**, 179-209.
8. S. Choudhary, *International journal of hydrogen energy*, 2012, **37**, 18713-18730.
9. N. Berkovitch, P. Ginzburg and M. Orenstein, *Journal of Physics: Condensed Matter*, 2012, **24**, 073202.
10. J.-H. Yun, Y. H. Ng, C. Ye, A. J. Mozer, G. G. Wallace and R. Amal, *ACS Applied Materials & Interfaces*, 2011, **3**, 1585-1593.
11. X. Han, Q. Kuang, M. Jin, Z. Xie and L. Zheng, *J. Am. Chem. Soc.*, 2009, **131**, 3152-3153.
12. Y. Bai, Z. Xing, H. Yu, Z. Li, R. Amal and L. Wang, *ACS Applied Materials & Interfaces*, 2013, **5**, 12058-12065.
13. A. Paracchino, V. Laporte, K. Sivula, M. Grätzel and E. Thimsen, *Nat Mater*, 2011, **10**, 456-461.
14. L. Li, L. Xu, W. Shi and J. Guan, *International Journal of Hydrogen Energy*, 2013, **38**, 816-822.
15. M. Hara, T. Kondo, M. Komoda, S. Ikeda, J. N. Kondo, K. Domen, M. Hara, K. Shinohara and A. Tanaka, *Chemical communications*, 1998, 357-358.
16. K. Lalitha, G. Sadanandam, V. D. Kumari, M. Subrahmanyam, B. Sreedhar and N. Y. Hebalkar, *The Journal of Physical Chemistry C*, 2010, **114**, 22181-22189.
17. M. Ichimura and Y. Kato, *Materials Science in Semiconductor Processing*, 2013, **16**, 1538-1541.
18. S. Choudhary, S. Upadhyay, P. Kumar, N. Singh, V. R. Satsangi, R. Shrivastav and S. Dass, *International Journal of Hydrogen Energy*, 2012, **37**, 18713-18730.
19. M. L. Personick, M. R. Langille, J. Zhang and C. A. Mirkin, *Nano Letters*, 2011, **11**, 3394-3398.
20. J. Zhang, M. R. Langille, M. L. Personick, K. Zhang, S. Li and C. A. Mirkin, *J. Am. Chem. Soc.*, 2010, **132**, 14012-14014.
21. T. Butburee, Y. Bai, J. Pan, X. Zong, C. Sun and G. Liu, L. Wang, *Journal of Materials Chemistry A*, 2014.
22. Q. T. Du, J. S. Tan, Q. T. Wang, C. Y. Li, X. H. Liu, R. S. Cai, Y. H. Ding and Y. Q. Wang, *Journal of Analytical Methods in Chemistry*, 2012, **2012**, 406162.
23. E. Thimsen, F. Le Formal, M. Grätzel and S. C. Warren, *Nano Letters*, 2010, **11**, 35-43.
24. F. Su, T. Wang, R. Lv, J. Zhang, P. Zhang, J. Lu and J. Gong, *Nanoscale*, 2013, **5**, 9001-9009.
25. Q. Wang, T. Butburee, X. Wu, H. Chen, G. Liu and L. Wang, *Journal of Materials Chemistry A*, 2013, **1**, 13524-13531.
26. K. Yu, Y. Tian and T. Tatsuma, *Physical Chemistry Chemical Physics*, 2006, **8**, 5417-5420.
27. W. Wang, S. Chen, P.-X. Yang, C.-G. Duan and L.-W. Wang, *Journal of Materials Chemistry A*, 2013, **1**, 1078-1085.
28. R. H. Coridan, M. Shaner, C. Wiggenhorn, B. S. Brunschwig and N. S. Lewis, *The Journal of Physical Chemistry C*, 2013, **117**, 6949-6957.
29. W. Siripala, A. Ivanovskaya, T. F. Jaramillo, S.-H. Baeck and E. W. McFarland, *Solar Energy Materials and Solar Cells*, 2003, **77**, 229-237.
30. Z. Luo, H. Jiang, D. Li, L. Hu, W. Geng, P. Wei and P. Ouyang, *RSC Advances*, 2014, **4**, 17797-17804.
31. P. Yang, J. Zhao, J. Wang, B. Cao, L. Li and Z. Zhu, *Journal of Materials Chemistry A*, 2015, **3**, 8256-8259.

32.   Y. Tachibana, L. Vayssieres and J. R. Durrant, *Nat Photon*, 2012, **6**, 511-518.

33.   L. Huang, F. Peng, H. Yu and H. Wang, *Solid State Sciences*, 2009, **11**, 129-138.